Cell Reports
Methods

Report

Cryosectioning and immunofluorescence of *C. elegans* reveals endogenous polyphosphate in intestinal endo-lysosomal organelles

Graphical abstract

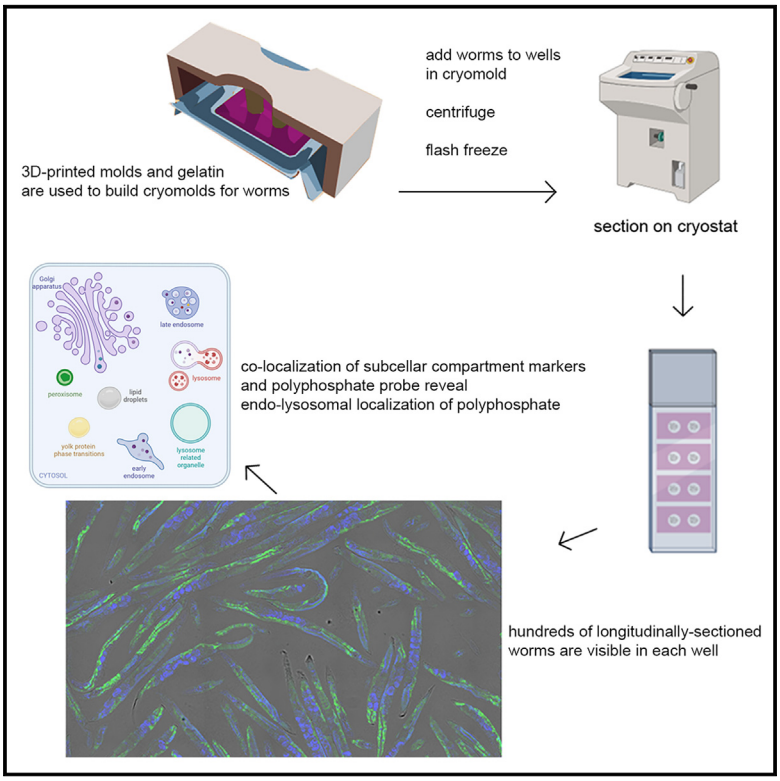

Highlights

- The cuticle of *Caenorhabditis elegans* has long hampered fluorescent staining approaches
- This cryosection method allows staining of hundreds of worms in a single experiment
- Staining for polyphosphate reveals its presence in endo-lysosomal compartments
- Polyphosphate levels are sensitive to food availability

Authors

Ellen Quarles, Lauren Petreanu, Anjali Narain, ..., Joyful Wang, Bryndon Oleson, Ursula Jakob

Correspondence

equarles@gmail.com

In brief

Polyphosphate (polyP), a ubiquitous and highly conserved molecule, is present throughout all branches of life yet has mostly been studied in single cells. Quarles et al. describe a method to longitudinally section *Caenorhabditis elegans*, allowing high-throughput staining of worms using polyP-specific fluorescent probes. These studies establish *C. elegans* as a model for polyP research.

Quarles et al., 2024, Cell Reports Methods *4*, 100879
October 21, 2024
https://doi.org/10.1016/j.crmeth.2024.100879

CellPress

Cell Reports Methods

CellPress
OPEN ACCESS

Report

Cryosectioning and immunofluorescence of *C. elegans* reveals endogenous polyphosphate in intestinal endo-lysosomal organelles

Ellen Quarles,[1,2,*] Lauren Petreanu,[1] Anjali Narain,[1] Aanchal Jain,[1] Akash Rai,[1] Joyful Wang,[1] Bryndon Oleson,[1] and Ursula Jakob[1]

[1]University of Michigan, Molecular, Cellular, and Developmental Biology Department, Ann Arbor, MI, USA
[2]Lead contact
*Correspondence: equarles@gmail.com
https://doi.org/10.1016/j.crmeth.2024.100879

MOTIVATION *Caenorhabditis elegans* are a widely used system to study basic biological phenomena. However, studies requiring fluorescently tagged molecules are restricted to genetically manipulated organisms or low-throughput and disruptive staining techniques, in part due to the presence of a tough cuticle. Labeling polyphosphate with known probes is not compatible with either of these options in a high-throughput setting. Thus, we describe a method to cryosection worms longitudinally and en masse to allow for staining with fluorescent probes with minimal chemical perturbation of the samples.

SUMMARY

Polyphosphate (polyP) is a ubiquitous polyanion present throughout the tree of life. While polyP's widely varied functions have been interrogated in single-celled organisms, little is known about the cellular distribution and function of polyP in multicellular organisms. To study polyP in metazoans, we developed the nematode *Caenorhabditis elegans* as a model system. We designed a high-throughput, longitudinal-orientation cryosectioning method that allowed us to scrutinize the intracellular localization of polyP in fixed *C. elegans* using fluorescent polyP probes and co-immunostaining targeting appropriate marker proteins. We discovered that the vast majority of polyP is localized within the endo-lysosomal compartments of the intestinal cells and is highly sensitive toward the disruption of endo-lysosomal compartment generation and food availability. This study lays the groundwork for further mechanistic research of polyPs in multicellular organisms and provides a reliable method for immunostaining hundreds of fixed worms in a single experiment.

INTRODUCTION

Polyphosphate (polyP), a simple polyanion composed of orthophosphates linked by high-energy phosphoanhydride bonds, is ubiquitously present throughout the tree of life. Its known functions vary wildly, depending on the organism, tissue, and cellular context.[1,2] PolyP is currently best understood in single-celled organisms,[3] particularly bacteria and budding yeast. This is largely due to the fact that in these organisms, the enzymes that make polyP (i.e., bacterial polyphosphate kinase [PPK], yeast Vtc4) and break the polymer (bacterial and yeast exopolyphosphatase [PPX]) have been identified and allow for genetic interrogations of polyP functions *in vivo*.[4] In contrast, the mammalian polyP synthesizing machinery remains unknown, and polyphosphatases of the Nudix protein family have only recently been discovered.[5] Moreover, while it is well known that polyP fulfills a multitude of different functions in higher eukaryotic cells, ranging from blood clotting[6] and neuronal glial signaling[7] to neurodegenerative diseases[8–10] and cancer,[11,12] model systems to study polyP in a multicellular and multi-tissue context are still lacking. In fact, even extracting polyP from multicellular organisms remains a major challenge due to the orders-of-magnitude lower abundance of polyP in mammalian cells and tissues compared to the millimolar concentrations of polyP that accumulate in environmentally stressed bacteria[13] or in the vacuole of *Saccharomyces cerevisiae*.[14] Nevertheless, visualization of polyP has been made possible in fixed tissues by using a probe consisting of the polyP-binding domain of *Escherichia coli* PPX fused with EGFP or mCherry (*Ec*PPXbd-EGFP and *Ec*PPXbd-mCherry, respectively), which binds long-chain polyP specifically.[15,16]

Our primary goal for this study was to assess and visualize the amount and (sub)cellular distribution of polyP in a multicellular organism. To do this, we chose *Caenorhabditis elegans* for its relative anatomical simplicity, its cost effectiveness, the abundance of available transgenic strains, and the ease with which knockdown experiments can be conducted. However, staining

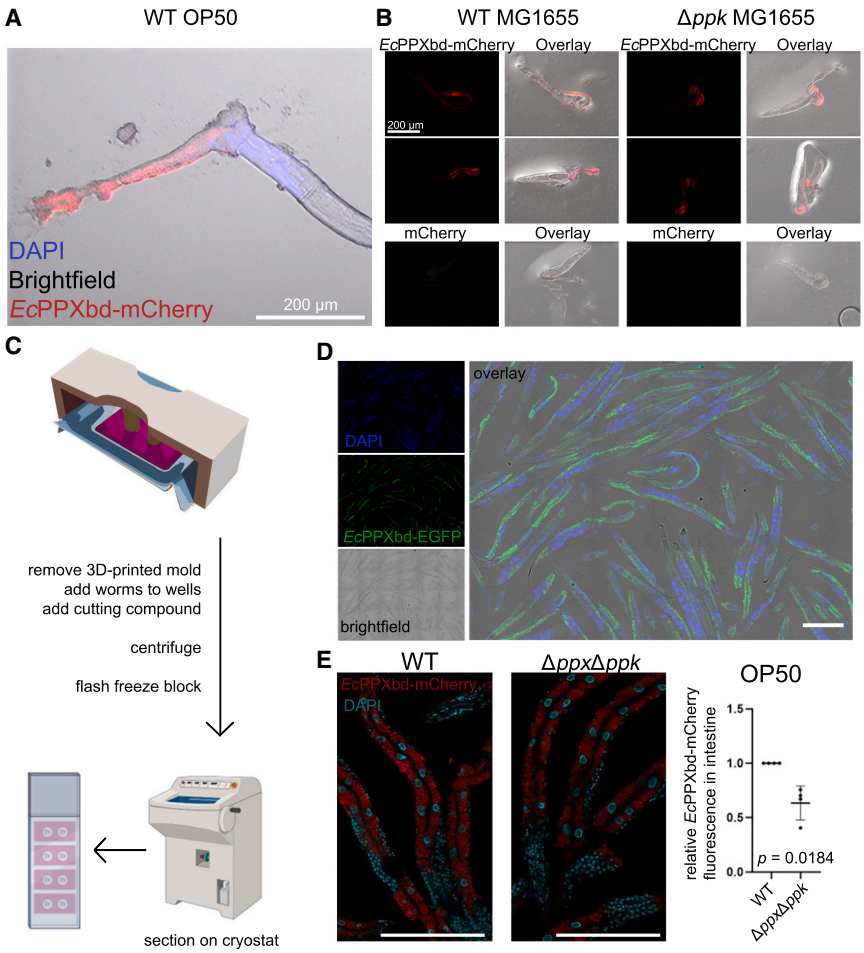

Figure 1. Visualization of *C. elegans* tissues reveals endogenous polyP

(A) A representative dissected adult N2 worm stained with *Ec*PPXbd-mCherry and DAPI and the differential interference contrast (DIC) image, shown in overlay.

(B) Similar images to those in (A): intestinal and gonadal tissue dissected from N2 adults and stained with *Ec*PPXbd-mCherry. The worms were raised on either wild-type MG1655 *E. coli* or a *ppk* deletion mutant. Bottom row: worms were stained with mCherry alone. Higher-resolution images are shown in Figure S1.

(C) Overview illustration of cryoblocking protocol.

(D) Representative image of adult worms stained with DAPI and *Ec*PPXbd-EGFP showing full body lengths of sectioned adjacent worms.

(E) Left: Z-projections of three 10 µm sections of adult N2s stained with *Ec*PPXbd-mCherry (pseudocolored red) and DAPI (pseudocolored teal) and fed either wild-type or *ppk/ppx* knockout OP50 bacteria. Right: graph of relative *Ec*PPXbd-mCherry fluorescent signal in intestines of worms fed either strain of bacteria (mean +/− SD). All scale bars represent 200 µm.

of polyP with the *Ec*PPXbd-EGFP probe posed a major challenge in *C. elegans* since antibody staining is notoriously difficult in whole worms.[17] The primary challenge is the presence of their cuticle, a biological fortress that protects the worms from the insults of the outside world. To gain access to the inner tissues requires chemical or mechanical disruption,[17] which is highly destructive to the structural components of the cell (chemical methods, dissection), only doable with very low throughput (dissection, freeze cracking), causes a high degree of technical error (dissection, freeze cracking), or requires chemicals that might compromise extraction and visualization efforts (chemical methods).[18] Hence, immunofluorescence (IF) on fixed *C. elegans* using commercially available antibodies, of which there are few that are optimized for worm proteins, is rarely performed. To address this issue, we considered using cryosectioning,[19] a method that is frequently performed with dissected tissues. The benefits of sectioning cryopreserved tissues include the low cost and technical ease of making the frozen blocks, the excellent antigenicity retained in the sections, and the possibility of long-term storage at −80°C. The challenge, however, lies in manipulating the position and orientation of small tissue sections or organisms such as worms within the same plane as the sectioning blade, given that wrong positioning will result in partial worm sections that make mapping that area back to the whole worm course-grained. We thus decided to develop a cryosectioning method using three-dimensional (3D)-printed molds that allow us to position hundreds of worms in the same plane, thus substantially increasing both the sample number and staining homogeneity. Our results indicate that *C. elegans* produce polyP endogenously, and, while polyP is contained in most tissues, the majority of worm polyP accumulates in endo-lysosomal vesicles in the intestine. Moreover, we demonstrate that this technique is a highly reliable tool for the immunostaining of hundreds of fixed worms in a single experiment, a useful addition to the *C. elegans* toolbox.

RESULTS AND DISCUSSION

Visualization of endogenous polyP in *C. elegans*

As a first approach to determine if *C. elegans* contain any visualizable polyP, we used a conventional dissection method in which the worm cuticle is nicked, allowing the extrusion of the gonad and intestine.[20] We then stained the dissected worms with *Ec*PPXbd-mCherry, which has been shown to specifically interact with polyP in fixed tissues.[15] As shown in Figure 1A, we observed a clear mCherry signal in the intestine, providing the first evidence that polyP can indeed be detected within select tissues of *C. elegans*. However, since the food source of *C. elegans* is *E. coli*, which produces ample amounts of polyP, we wondered whether the intestinal polyP signal might originate from the ingested bacteria. To test this idea, we cultivated the worms on either wild-type (WT) *E. coli* MG1655 or the *ppk*

deletion mutant, which fails to produce any polyP.[21] We did not observe any obvious differences in the intensity of the *Ec*PPXbd-mCherry signal in the intestines of worms grown on either of the bacteria, making us confident that *C. elegans* is indeed able to synthesize polyP (Figures 1B and S1A). Nonetheless, these studies also made us realize that the data analysis of these dissection images is extremely difficult due to the considerable variability in tissue integrity and completeness of the dissections. Moreover, by using DAPI co-staining, we noticed that even this highly penetrant stain only occasionally permeated tissues more than one or two cells deep into areas where the cuticle was damaged. We thus concluded that while this method allowed us to confirm the presence of endogenous polyP in *C. elegans*, it was insufficient to provide meaningful data about the subcellular distribution of polyP or its presence in parts of the worms from which the cuticle could not be removed.

Establishing a high-throughput cryosectioning technique for *C. elegans*

To improve the technical consistency in opening the cuticles and accessing all worm tissues as well as increasing the throughput and reproducibility of stained and imaged worms, we decided to develop a higher-throughput cryosectioning approach (Figures 1C and S2). Cryosectioning, which is employed in pathology labs around the world,[19] involves the dissection of tissues, addition of a liquid cutting compound, arrangement of the tissue pieces into the preferred orientation using forceps, and flash freezing of the samples. However, the proper arrangements of worms in the same plane for cryosectioning, which is necessary to obtain full-length worm sections rather than circular or oval cross-sections, is technically very challenging and likely the major factor why this method has not yet been developed for *C. elegans*. Previous cryosectioning attempts in worms were restricted to individual nematodes and used to specifically isolate cross-sections for RNA isolation.[22,23] To achieve the longitudinal alignment of several hundred worms in each sample, we designed and 3D-printed 2- to 18-well gelatin molds, which could be centrifuged to align the optimal cutting temperature (OCT; a freezing compound routinely used for preparing cryosamples)-treated worms at the bottom of the wells. After freezing the resulting blocks, we then generated sections using the cryostat (Figures 1C and S2). Since adult *C. elegans* are about 80 μm thick, taking several slices at 10–12 μm thickness allows for multiple sections of the same worms to be added to one or more slides. By using blocks with up to 18 wells, this setup allowed us to minimize variation in the staining from slide to slide by staining sections from the same population on separate slides, staining multiple populations on the same slide, or both. By applying this method and subsequently staining the sections using either *Ec*PPXbd-EGFP or *Ec*PPXbd-mCherry together with DAPI, we were able to image hundreds of worms in a single experiment at high resolution (Figure 1D). To quantitatively describe the potential effects of bacterial polyP on the *Ec*PPXbd-mCherry signal in the worm intestines, we also compared worms fed on WT bacteria versus those lacking both *ppx* and *ppk* (OP50$^{\Delta PPK\Delta PPX}$) (Figure 1E). These experiments revealed a slight but reproducible decrease in the *Ec*PPXbd-mCherry signal in the mutant OP50-fed worms, suggesting that while worms produce most of their own polyP, the food source can contribute to intestinal polyP levels. As before, we observed the strongest *Ec*PPXbd-mCherry signal in the intestines of the worms. Importantly, this signal was completely lost upon pretreatment of the sections with *S. cerevisiae* PPX (*Sc*PPX) and increased upon treatment with the endopolyphospatase DPP1, which cleaves polyP chains and thus increases the number of polyP termini, the site of polyP hydrolysis by PPX[24] (Figures S3A and S3B). Combined treatment with both PPX and DPP1 re-reduced the signal although not to the full extent of the treatment with PPX alone. Since PPX is a processive enzyme with a chain length limit (~15 residues),[25] it is conceivable that DPP1 produces some polyP chains that are too short for PPX to be further hydrolyzed. Moreover, staining with mCherry alone only gave very faint non-specific background staining. These results not only demonstrated that we developed a tool that, for the first time, allows us and others to immunostain entire fixed *C. elegans* worms in a high-throughput manner but also provided further evidence that we can visualize endogenous polyP in a multicellular organism.

Tissue-wide and subcellular distribution of polyP in *C. elegans*

Now that we generated a technique that provided accessibility of all worm tissues to the stain, we took a more granular look at the polyP distribution in *C. elegans* (Figure 2A). While the most prominent polyP signal was found in the intestine, *Ec*PPXbd-EGFP signals significantly above the EGFP background signal were distributed throughout the entire worm body (Figure 2A). Apart from the intestinal cells, we found polyP to be present in the gonad and to diffuse staining through the body wall and head. Due to the ease of separating their signals from surrounding tissues on the images, we analyzed three separate tissues—the head region, the gonad (pachytene and oocytes), and the intestinal cells (Figure 2B). The pachytene is an acellular space within the proximal gonad, chosen specifically because it had the brightest signal of the gonadal regions analyzed, with the least interference of signal from cellular spaces. As expected from the images, the head region and the gonadal areas showed much lower and more diffuse signals compared to the intestinal cells (Figure 2C), providing good evidence that the intestine indeed harbors the primary polyP stores in *C. elegans*. Since the brightest polyP signal was clearly in punctate structures in the gut, we focused on the intestinal polyP for the remainder of the study.

Intestinal polyP is most prominently located in endo-lysosome vesicles

Higher-resolution analysis of the stained worms revealed that the intestinal polyP signal appeared in round puncta, suggestive of its presence within distinct subcellular compartments. The ranges of sizes and shapes of the *Ec*PPXbd-EGFP/mCherry puncta potentially fit several known organelles and liquid-liquid phase condensates known to be present in the *C. elegans* gut (Figure 3, middle). To characterize the subcellular localization of polyP in more detail, we either used publicly available chromosome-encoded fluorophore-protein fusion worm strains or exploited our new-found ability to use commercially available antibodies and dyes to stain subcellular organelles

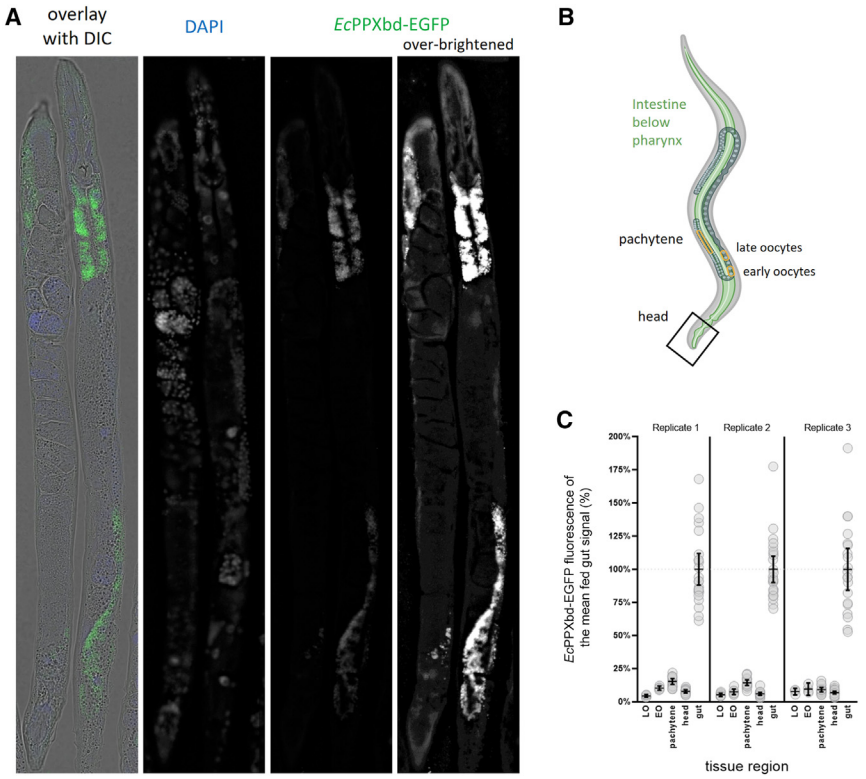

Figure 2. *C. elegans* polyP accumulates in intestinal cells

Worm sections for tissue- or region-specific differences in PPXbd-EGFP fluorescence were analyzed.

(A) Representative N2 adults at day 1, 10 μm sections, stained with DAPI and EcPPXbd-EGFP, which is shown at two different intensity levels to visualize gut and non-gut signals.

(B) Schematic of regions analyzed. The pachytene is the non-cellular region of the proximal gonad. Oocytes: (late: 1st and 2nd oocytes counting from the proximal end of the gonad before the spermatheca valve; early: 4th and 5th positions).

(C) Graph of background-corrected *Ec*PPXbd-EGFP fluorescence levels, normalized to mean intestinal signal within each worm (set to 100%), for each region in (A). Three replicate experiments are shown. Each point is one worm, and lines are mean ± SEM.

and liquid-liquid phase separations (LLPS) for which no fluorescently tagged worms strains were available. Our analysis of their potential co-localization with the *Ec*PPXbd-EGFP or *Ec*PPXbd-mCherry signal nicely illustrated that this cryosection technique is indeed a powerful method to detect, monitor, and quantify proteins and lipids in large numbers of fixed worms. We did not observe any co-localization of the *Ec*PPXbd-mCherry signal with a fluorescently tagged Golgi membrane marker, which appears as a punctate structure in the *C. elegans* intestines,[26] a peroxisome membrane marker, or the yolk protein marker vitulin-2 fused to GFP (Figure 3A). Moreover, by using an antibody against *C. elegans* rme-1, a marker for recycling endosomes, we also ruled out the presence of polyP in those organelles (Figure S4). To determine if early endosomes contained polyP, we used a rab-5::GFP worm strain, which appeared to have a small number of very large compartments labeled with EGFP, indicating that the strain has a compromised endo-lysosomal system. Still, we did not observe *Ec*PPXbd-mCherry within these structures. We also did not observe any co-localization of *Ec*PPXbd-EGFP with lipid droplets, which we visualized via oil red O staining (Figure S4). Instead, we found very clear co-localization with membrane markers of lysosomes (lmp-1::GFP), late endosomes (rab-7::GFP), and so called "gut granules" (glo-1::GFP) (Figure 3, right). Gut granules are lysosome-related organelles (LROs) specific to the worm intestine.[27] In each of these vesicles, the *Ec*PPXbd-EGFP signal was surrounded by membrane marker fluorescence, indicating that the polyP resides inside these vesicles. This result was particularly noteworthy because polyP has previously been observed to accumulate in cell-type-specific LROs, such as acidocalcisomes (also known as dense granules) in trypanosomes.[3] V-ATPases in the acidocalcisome membrane have been suggested to be critical for polyP synthesis and transport in trypanosomes and other eukaryotes.[28] *C. elegans* lysosomes, late endosomes, and LROs are highly dynamic compartments, which merge with each other and other vesicles, sharing membrane components in the process.[29] Based on this reason, we are unable to conclusively state that polyP is only present in these specific compartments since other vesicles, such as the autophagosomes, share the same membrane markers, even if only temporarily. Nevertheless, these studies clearly demonstrated that polyP is a component of the endo-lysosomal system of vesicles. It is of note, however, that not every endo-lysosomally marked vesicle contained polyP and that not every polyP puncta co-localized with each specific membrane marker that we used. While we cannot rule out that other compartments outside of the endo-lysosomal system contain polyP, these results are consistent with polyP being spread throughout the endo-lysosomal system. In any case, however, these results suggested that polyP synthesis is likely coupled to the development of endo-lysosomal vesicles.

Disrupting endo-lysosomal vesicle development reduces polyP abundance

To monitor whether the synthesis of polyP is connected to endo-lysosomal vesicle development, we obtained worms that carried a mutation in the membrane protein lmp-1. These mutant worms have a greatly reduced number and size of lysosomes.[30] Indeed, cryosectioning and staining of the *lmp-1* knockout (KO) worms with *Ec*PPXbd-EGFP revealed a significant reduction in the number and size of the *Ec*PPXbd-EGFP^{+} vesicles compared to age-matched WT N2 worms (Figures 4A–4D). In worms defective in functional glo-1,[31] a protein that is involved in the formation of

CellPress
OPEN ACCESS

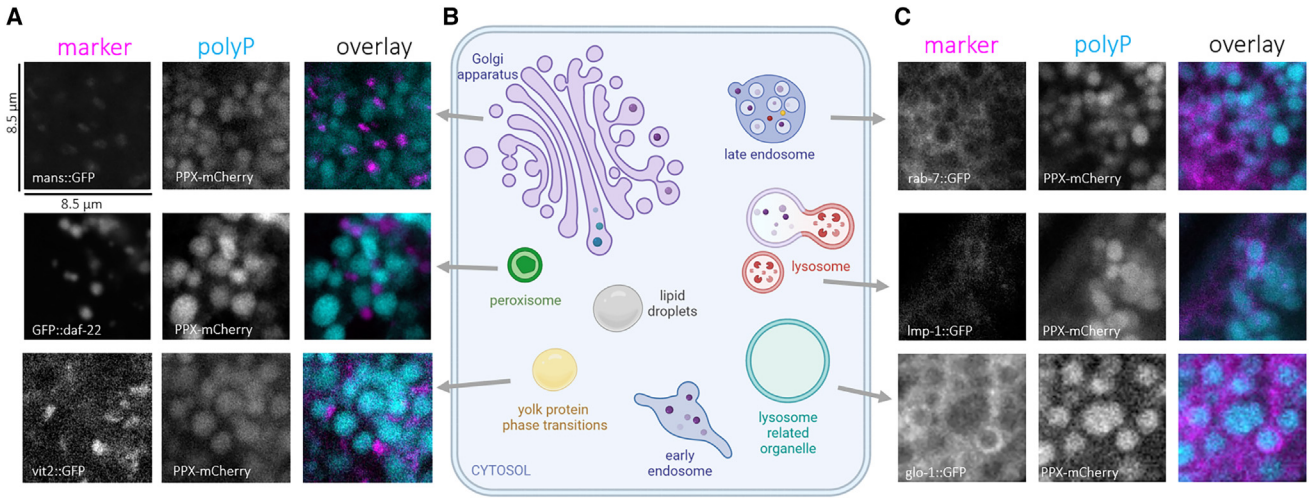

Figure 3. *Ec*PPXbd-mCherry-positive puncta are surrounded by membrane markers of endo-lysosomal vesicles

(A) Grayscale images of representative day 1 worm intestinal cells, expressing the listed markers of Golgi apparatus, peroxisomes, and yolk protein, stained with *Ec*PPXbd-mCherry and overlays.

(B) Cartoon of various subcellular compartments in which *Ec*PPXbd-mCherry co-localization was tested in this study prepared using BioRender (biorender.com).

(C) Same as in (A) but showing membrane marker signal surrounds *Ec*PPXbd-mCherry signal for markers of endosomes, lysosomes, and lysosome-related organelles. Scale bar represents 8.5 µm.

the gut granules, the dimmer and smaller vesicles were left intact, while the largest-diameter subset of *Ec*PPXbd-EGFP^{+} vesicles disappeared (Figures 4A–4D). These results and the observation that lmp-1^{KO} worms harbor the smallest population of polyP^{+} vesicles are consistent with previous research that showed that *lmp-1* KO worms have a severely reduced population of lysosomes as well as a loss of downstream endo-lysosomal compartments, including gut granules.[30] These results strongly suggest that polyP synthesis and its accumulation are coupled to the biogenesis of lysosomes in *C. elegans*. We also investigated the *Ec*PPXbd-EGFP signal in the heads of the mutant worms and found no difference between N2, glo-1^{KO}, and lmp-1^{KO} worms (Figure S5). These results indicate that polyP levels in the head regions of the worms that are detectable with our *Ec*PPXbd-EGFP probe are not dependent on intestine-specific lmp-1- or glo-1-containing organelles. The origin and maintenance of that pool of polyP requires further study.

Transient starvation depletes polyP stores from endo-lysosomal vesicles

PolyP has long been thought to act as an energy reservoir, allowing for the storage of high-energy phosphoanhydride bonds while keeping the osmotic burden at a minimum.[32] We now wondered whether worms utilize the endo-lysosomal polyP stores as an energy source under food-poor conditions. To test this, we grew N2 worms to day 1 of adulthood and then transferred them onto fresh plates containing either OP50 WT bacteria or no bacteria. After 4 h of starvation, we either directly collected the worms for cryosectioning or transferred the starved worms onto OP50^{WT}-containing plates for an additional 1, 2, 4, or 24 h before cryoblocking and analysis. As shown in Figure 4E, we found that the *Ec*PPXbd-EGFP signal in the intestine dropped significantly within 4 h of food starvation. At this point, it is unclear whether polyP is converted back to ATP, transported elsewhere, or capped at the ends, which could render it invisible to *Ec*PPXbd-EGFP. However, since the *Ec*PPXbd-EGFP signal slowly returned upon the re-introduction of food, it is most likely that polyP stores are being depleted during starvation and filled up again as soon as food becomes re-available. We hypothesized that the depletion of polyP would occur throughout the entire worm tissues and, indeed, found a significant drop in polyP levels also in the head region of the worm, which was recovered upon the re-introduction of food (Figure 3F). The reduction in signal was not as dramatic as compared to the intestine, suggesting there is a difference in the dynamics of loss in this polyP pool.

In summary, our study adds a metazoan model to the polyP field, allowing the visualization and manipulation of endogenous polyP and forming the groundwork for future mechanistic studies on the cross-tissue control of polyP. At this point, we do not yet understand what is happening to the sources of polyP during starvation and how polyP stores are refilled upon food availability. Is polyP exported as a whole chain or broken down into orthophosphate units, and how are they exported from the vesicles? It may also be the case that the ends of the polyP chains are simply made unavailable to *Ec*PPXbd-EGFP through some hitherto unknown binding event, which may render it invisible to our IF method.[33] We do not know how polyP distributes in non-intestinal cells since all of our transgenic lines marking those intracellular compartments are intestine-specific. There are many potential areas of study now available, and we expect that our longitudinally-oriented cryosectioning method will open the door for more worm researchers to investigate polyP in this organism. Our method for sectioning hundreds of worms in different conditions simultaneously is a powerful tool for *C. elegans* research. For most protein localization work in

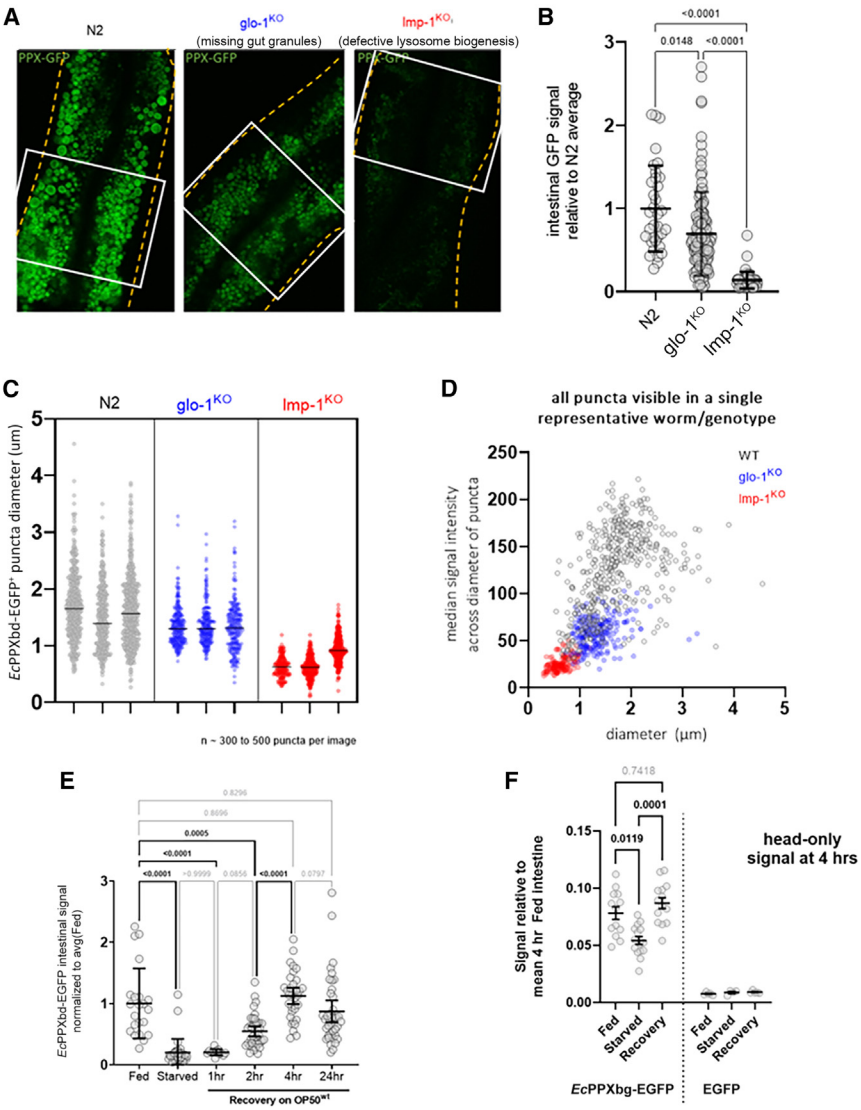

Figure 4. Gut *Ec*PPXbd-EGFP signal is dependent on endo-lysosomal vesicle formation and food availability

(A) Representative images of N2, glo-1^{KO}, and lmp-1^{KO} day 1 adults stained with *Ec*PPXbd-EGFP. Cuticle of worm is denoted by a dashed yellow line. Area used for fluorescence measurement in Figure 3B is shown with a white rectangle. Scale bar represents 20 μm.

(B) Relative fluorescence of *Ec*PPXbd-EGFP signal in intestine. Each circle is one worm. Kruskal-Wallis test with Dunn's post hoc was used. Error bars are mean +/− SD.

(C) Quantification of diameter of *Ec*PPXbd-EGFP-positive puncta in three representative images from 3 separate worms of intestinal cells. Bar = median. Each dot is one punctum.

(D) Graph of signal intensity of each puncta by its diameter. Each circle is one punctum.

(E) Quantification of *Ec*PPXbd-EGFP before and after food removal and recovery. Each dot represents one worm. Kruskal-Wallis test with Dunn's post hoc was used. *p* value is shown for each comparison made. Error bars are mean +/− SEM.

(F) Relative fluorescence of *Ec*PPXbd-EGFP signal in the heads of worms relative to the fed 4 h intestinal signal. Each circle is one worm. Kruskal-Wallis test with Dunn's post hoc was used. Lines are mean ± SEM. *p* value is shown for each comparison made. All comparisons between GFP only groups had $p > 0.4$.

C. elegans, researchers depended on the use of transgenic animals expressing fluorophore-fused native proteins. While this is a powerful system for studying proteins in live animals, it may alter the localization and activity of the fusion proteins. Moreover, each of these strains takes months to make, significantly increasing the costs of this research. Our method is inexpensive, fast, and highly reproducible. Moreover, since many of the established antibodies cross-react with worm proteins, we are convinced that this 3D-printed-well and cryosectioning method will be a welcome addition to the *C. elegans* toolbox.

Limitations of the study

We currently have no way of verifying that all of the polyP in the samples is retained after sample processing. Therefore, even if the fluorescent probe is detecting all available polyP, we cannot say for certain that all biologically important pools of polyP are visualizable using this method. It is unlikely that an abundant reservoir is missing due to the similar pattern of the *Ec*PPXbd-mCherry signal in freeze-cracked versus cryosectioned worms.

When using the freeze-cracking method to prepare *C. elegans* samples for IF, the entirety of the worm is present on the slide. However, by using cryosectioning to bypass the cuticle, there will always be missing parts of each worm that is sectioned. Another limitation of sectioning is related to imaging: thinner sample sections (8–12 μm) will be easier to image clearly than thicker samples, which have more tissue to image through. Thicker samples will include more spatial information in the whole organism, which allows for easier identification of various tissues.

There are few probes for polyP in the literature. While the one we employed for this study is well verified as polyP-specific in mammalian cells,[16] it is possible that the probe was unable to bind and fluoresce in all polyP pools in the samples. Further validation could include genetic manipulation of the *C. elegans* to express an PPX from bacteria to the gut granules specifically and observe a loss of *Ec*PPXbd-EGFP staining. Alternatively, creating a non-binding version of this probe would be an excellent control for specificity in a *C. elegans* system.

RESOURCE AVAILABILITY

Lead contact

Further information and requests for resources and reagents should be directed to and will be fulfilled by the lead contact, Ellen Quarles (equarles@gmail.com).

Materials availability

3D model files of the pronged molds and centrifuge adaptors are available in several formats. Contact Ellen Quarles for the files. If users are unable to print these files themselves, we recommend using a service such as Shapeways.com. Strains used in this paper are available upon request from the Jakob lab at the University of Michigan by contacting Ursula Jakob (ujakob@umich.edu).

Data and code availability

- The data reported in this paper are available from the lead contact upon request.
- This study does not report original code.
- Any further information required to re-analyze the data reported in this paper is available from the lead contact upon request.

ACKNOWLEDGMENTS

We thank Ken Wan for purifying the proteins, Traci Banjanin for preparing many of the materials used for the study, and James Bardwell (University of Michigan) for access to the Leica Thunder microscope. We also thank Gregg Sobocinski for his help and expertise with microscopy. We are thankful for the following funding: the Michigan Society of Fellows (E.Q.), a BrightFocus ADR Fellowship (A2019250F to B.O.), and a University of Michigan T32-AG000114 Career Training in the Biology of Aging Training Grant (to B.O.) Funding for the study came from National Institutes of Health grant GM122506 (to U.J.).

AUTHOR CONTRIBUTIONS

Conceptualization, E.Q. and U.J.; methodology, E.Q.; validation, E.Q., L.P., A.N., A.J., and J.W.; formal analysis, E.Q.; investigation, E.Q., B.O., A.R., L.P., A.N., A.J., and J.W.; resources, E.Q. and U.J.; writing – original draft, E.Q.; writing – review & editing, U.J.; visualization, E.Q., B.O., and A.R.; supervision, E.Q. and U.J.; funding acquisition, U.J.

DECLARATION OF INTERESTS

The authors declare no competing interests.

STAR★METHODS

Detailed methods are provided in the online version of this paper and include the following:

- KEY RESOURCES TABLE
- EXPERIMENTAL MODEL AND STUDY PARTICIPANT DETAILS
  - Strains
  - Culturing *C. elegans*
- METHOD DETAILS
  - Preparation of cryomolds
  - Freezing worms in cryomolds
  - Cryosectioning
  - Purification of fluorescent probes, ScPPX and DPP1
  - Staining and immunofluorescence
  - Fluorescence microscopy
  - Measurement of fluorescence intensity
  - Food removal and recovery
  - Enzyme digestion used in Figure S3
- QUANTIFICATION AND STATISTICAL ANALYSIS

SUPPLEMENTAL INFORMATION

Supplemental information can be found online at https://doi.org/10.1016/j.crmeth.2024.100879.

Received: August 11, 2023
Revised: June 11, 2024
Accepted: September 20, 2024
Published: October 15, 2024

REFERENCES

1. Kornberg, A., Rao, N.N., and Ault-Riché, D. (1999). Inorganic Polyphosphate: A Molecule of Many Functions. Annu. Rev. Biochem. *68*, 89–125. https://doi.org/10.1146/annurev.biochem.68.1.89.
2. Bowlin, M.Q., and Gray, M.J. (2021). Inorganic polyphosphate in host and microbe biology. Trends Microbiol. *29*, 1013–1023. https://doi.org/10.1016/j.tim.2021.02.002.
3. Docampo, R., and Moreno, S.N. (1999). Acidocalcisome: A Novel Ca2+ Storage Compartment in Trypanosomatids and Apicomplexan Parasites. Parasitol. Today *15*, 443–448. https://doi.org/10.1016/s0169-4758(99)01531-8.
4. Denoncourt, A., and Downey, M. (2021). Model systems for studying polyphosphate biology: a focus on microorganisms. Curr. Genet. *67*, 331–346. https://doi.org/10.1007/s00294-020-01148-x.
5. Samper-Martín, B., Sarrias, A., Lázaro, B., Pérez-Montero, M., Rodríguez-Rodríguez, R., Ribeiro, M.P.C., Bañón, A., Wolfgeher, D., Jessen, H.J., Alsina, B., et al. (2021). Polyphosphate degradation by Nudt3-Zn2+ mediates oxidative stress response. Cell Rep. *37*, 110004. https://doi.org/10.1016/j.celrep.2021.110004.
6. Baker, C.J., Smith, S.A., and Morrissey, J.H. (2019). Polyphosphate in thrombosis, hemostasis, and inflammation. Res. Pract. Thromb. Haemost. *3*, 18–25. https://doi.org/10.1002/rth2.12162.
7. Holmström, K.M., Marina, N., Baev, A.Y., Wood, N.W., Gourine, A.V., and Abramov, A.Y. (2013). Signalling properties of inorganic polyphosphate in the mammalian brain. Nat. Commun. *4*, 1362. https://doi.org/10.1038/ncomms2364.
8. Lempart, J., and Jakob, U. (2019). Role of Polyphosphate in Amyloidogenic Processes. Cold Spring Harb. Perspect. Biol. *11*, a034041. https://doi.org/10.1101/cshperspect.a034041.
9. Arredondo, C., Cefaliello, C., Dyrda, A., Jury, N., Martinez, P., Díaz, I., Amaro, A., Tran, H., Morales, D., Pertusa, M., et al. (2022). Excessive release of inorganic polyphosphate by ALS/FTD astrocytes causes non-cell-autonomous toxicity to motoneurons. Neuron *110*, 1656–1670.e12. https://doi.org/10.1016/j.neuron.2022.02.010.
10. Borden, E.A., Furey, M., Gattone, N.J., Hambardikar, V.D., Liang, X.H., Scoma, E.R., Abou Samra, A., D-Gary, L.R., Dennis, D.J., Fricker, D., et al. (2021). Is there a link between inorganic polyphosphate (polyP), mitochondria, and neurodegeneration? Pharmacol. Res. *163*, 105211. https://doi.org/10.1016/j.phrs.2020.105211.
11. Shim, Y.J., Chatterjee, V., Swaidani, S., Alluri, R.K., Kundu, S., Merkulova, A., Angelini, D., You, D., Whitney, S.A., Feener, E.P., et al. (2021). Polyphosphate expression by cancer cell extracellular vesicles mediates binding of factor XII and contact activation. Blood Adv. *5*, 4741–4751. https://doi.org/10.1182/bloodadvances.2021005116.
12. Kulakovskaya, E.V., Zemskova, M.Y., and Kulakovskaya, T.V. (2018). Inorganic Polyphosphate and Cancer. Biochemistry. *83*, 961–968. https://doi.org/10.1134/s0006297918080072.
13. Gray, M.J. (2019). Inorganic Polyphosphate Accumulation in Escherichia coli Is Regulated by DksA but Not by (p)ppGpp. J. Bacteriol. *201*, e00664-18. https://doi.org/10.1128/JB.00664-18.
14. Breus, N.A., Ryazanova, L.P., Suzina, N.E., Kulakovskaya, N.V., Valiakhmetov, A.Y., Yashin, V.A., Sorokin, V.V., and Kulaev, I.S. (2011). Accumulation of inorganic polyphosphates in Saccharomyces cerevisiae under nitrogen deprivation: Stimulation by magnesium ions and peculiarities of localization. Microbiology *80*, 624–630. https://doi.org/10.1134/s002626171105002x.
15. Saito, K., Ohtomo, R., Kuga-Uetake, Y., Aono, T., and Saito, M. (2005). Direct labeling of polyphosphate at the ultrastructural level in Saccharomyces cerevisiae by using the affinity of the polyphosphate binding

domain of Escherichia coli exopolyphosphatase. Appl. Environ. Microbiol. *71*, 5692–5701. https://doi.org/10.1128/AEM.71.10.5692-5701.2005.

16. Borghi, F., Azevedo, C., Johnson, E., Burden, J.J., and Saiardi, A. (2024). A mammalian model reveals inorganic polyphosphate channeling into the nucleolus and induction of a hyper-condensate state. Cell Rep. Methods *4*, 100814. https://doi.org/10.1016/j.crmeth.2024.100814.
17. Duerr, J.S. (2013). Antibody Staining in C. Elegans Using "Freeze-Cracking". J. Vis. Exp. https://doi.org/10.3791/50664-v.
18. Duerr, J.S. (2006). Immunohistochemistry. WormBook: the online review of C. elegans biology. WormBook. https://doi.org/10.1895/wormbook.1.105.1.
19. Ross, M.A., Kohut, L., and Loughran, P.A. (2022). Cryosectioning. Curr. Protoc. *2*, e342. https://doi.org/10.1002/cpz1.342.
20. Crittenden, S.L., Troemel, E.R., Evans, T.C., and Kimble, J. (1994). GLP-1 is localized to the mitotic region of the C. elegans germ line. Development *120*, 2901–2911. https://doi.org/10.1242/dev.120.10.2901.
21. Gray, M.J., Wholey, W.Y., Wagner, N.O., Cremers, C.M., Mueller-Schickert, A., Hock, N.T., Krieger, A.G., Smith, E.M., Bender, R.A., Bardwell, J.C.A., and Jakob, U. (2014). Polyphosphate Is a Primordial Chaperone. Mol. Cell *53*, 689–699. https://doi.org/10.1016/j.molcel.2014.01.012.
22. Ebbing, A., Vértesy, Á., Betist, M.C., Spanjaard, B., Junker, J.P., Berezikov, E., van Oudenaarden, A., and Korswagen, H.C. (2018). Spatial Transcriptomics of C. elegans Males and Hermaphrodites Identifies Sex-Specific Differences in Gene Expression Patterns. Dev. Cell *47*, 801–813.e6. https://doi.org/10.1016/j.devcel.2018.10.016.
23. Rödelsperger, C., Ebbing, A., Sharma, D.R., Okumura, M., Sommer, R.J., and Korswagen, H.C. (2021). Spatial Transcriptomics of Nematodes Identifies Sperm Cells as a Source of Genomic Novelty and Rapid Evolution. Mol. Biol. Evol. *38*, 229–243. https://doi.org/10.1093/molbev/msaa207.
24. Lonetti, A., Szijgyarto, Z., Bosch, D., Loss, O., Azevedo, C., and Saiardi, A. (2011). Identification of an evolutionarily conserved family of inorganic polyphosphate endopolyphosphatases. J. Biol. Chem. *286*, 31966–31974. https://doi.org/10.1074/jbc.M111.266320.
25. Akiyama, M., Crooke, E., and Kornberg, A. (1993). An exopolyphosphatase of Escherichia coli. The enzyme and its ppx gene in a polyphosphate operon. J. Biol. Chem. *268*, 633–639.
26. Sato, M., Saegusa, K., Sato, K., Hara, T., Harada, A., and Sato, K. (2011). Caenorhabditis elegans SNAP-29 is required for organellar integrity of the endomembrane system and general exocytosis in intestinal epithelial cells. Mol. Biol. Cell *22*, 2579–2587. https://doi.org/10.1091/mbc.E11-04-0279.
27. Morris, C., Foster, O.K., Handa, S., Peloza, K., Voss, L., Somhegyi, H., Jian, Y., Vo, M.V., Harp, M., Rambo, F.M., et al. (2018). Function and regulation of the Caenorhabditis elegans Rab32 family member GLO-1 in lysosome-related organelle biogenesis. PLoS Genet. *14*, e1007772. https://doi.org/10.1371/journal.pgen.1007772.
28. Lander, N., Cordeiro, C., Huang, G., and Docampo, R. (2016). Polyphosphate and acidocalcisomes. Biochem. Soc. Trans. *44*, 1–6. https://doi.org/10.1042/BST20150193.
29. Delahaye, J.L., Foster, O.K., Vine, A., Saxton, D.S., Curtin, T.P., Somhegyi, H., Salesky, R., and Hermann, G.J. (2014). Caenorhabditis elegans HOPS and CCZ-1 mediate trafficking to lysosome-related organelles independently of RAB-7 and SAND-1. Mol. Biol. Cell *25*, 1073–1096. https://doi.org/10.1091/mbc.E13-09-0521.
30. Kostich, M., Fire, A., and Fambrough, D.M. (2000). Identification and molecular-genetic characterization of a LAMP/CD68-like protein from Caenorhabditis elegans. J. Cell Sci. *113*, 2595–2606. https://doi.org/10.1242/jcs.113.14.2595.
31. Hermann, G.J., Schroeder, L.K., Hieb, C.A., Kershner, A.M., Rabbitts, B.M., Fonarev, P., Grant, B.D., and Priess, J.R. (2005). Genetic analysis of lysosomal trafficking in Caenorhabditis elegans. Mol. Biol. Cell *16*, 3273–3288. https://doi.org/10.1091/mbc.e05-01-0060.
32. Xie, L., and Jakob, U. (2019). Inorganic polyphosphate, a multifunctional polyanionic protein scaffold. J. Biol. Chem. *294*, 2180–2190. https://doi.org/10.1074/jbc.REV118.002808.
33. Xie, L., Rajpurkar, A., Quarles, E., Taube, N., Rai, A.S., Erba, J., Sliwinski, B., Markowitz, M., Jakob, U., and Knoefler, D. (2019). Accumulation of Nucleolar Inorganic Polyphosphate Is a Cellular Response to Cisplatin-Induced Apoptosis. Front. Oncol. *9*, 1410. https://doi.org/10.3389/fonc.2019.01410.
34. Datsenko, K.A., and Wanner, B.L. (2000). One-step inactivation of chromosomal genes in Escherichia coli K-12 using PCR products. Proc. Natl. Acad. Sci. USA *97*, 6640–6645. https://doi.org/10.1073/pnas.120163297.
35. Blattner, F.R., Plunkett, G., 3rd, Bloch, C.A., Perna, N.T., Burland, V., Riley, M., Collado-Vides, J., Glasner, J.D., Rode, C.K., Mayhew, G.F., et al. (1997). The complete genome sequence of Escherichia coli K-12. Science *277*, 1453–1462. https://doi.org/10.1126/science.277.5331.1453.
36. Schindelin, J., Arganda-Carreras, I., Frise, E., Kaynig, V., Longair, M., Pietzsch, T., Preibisch, S., Rueden, C., Saalfeld, S., Schmid, B., et al. (2012). Fiji: an open-source platform for biological-image analysis. Nat. Methods *9*, 676–682. https://doi.org/10.1038/nmeth.2019.

STAR★METHODS

KEY RESOURCES TABLE

REAGENT or RESOURCE	SOURCE	IDENTIFIER
Chemicals, peptides, and recombinant proteins		
Gelatin, bovine	Sigma-Aldrich	G9391-100G
Phosphate buffered saline (no Mg^{2+}, no Ca^{2+})	Fisher Scientific	70-011-044
d-sucrose	Sigma-Aldrich	S9378
Paraformaldehyde, 8% solution	Electron Microscopy Sciences	157-8-100
Triton X-100	Sigma-Aldrich	T9284
O.C.T. (Optical Cutting Compound)	Fisher Scientific	23-730-571
*Ec*PPXbd-mCherry	This paper	
*Ec*PPXbd-eGFP	This paper	
mCherry	This paper	
eGFP	This paper	
Oil Red O	Sigma-Aldrich	O9755
Polypropylene glycol (100%)	MP Biomedicals, LLC	Catalog # 151957
Food coloring	McCormick	Assorted Food Color and Egg Dye
Antibodies		
Anti-LMP-1	Developmental Studies Hybridoma Bank (https://dshb.biology.uiowa.edu/) LMP1 was deposited to the DSHB by Nonet, M.L./Hadwiger, G./Dour, S.	LMP1, RRID: AB_2161795
Anti-RME-1	Developmental Studies Hybridoma Bank (https://dshb.biology.uiowa.edu/) RME1 was deposited to the DSHB by Nonet, M.L./Hadwiger, G./Dour, S.	RME1, RRID: AB_10571460
Experimental models: Organisms/strains		
N2 (Bristol)	Caenorhabditis Genetics Center	N2
Glo-1^{KO} (glo-1(zu391))	Caenorhabditis Genetics Center	JJ1271
Lmp-1^{KO} (lmp-1(nr2045))	Caenorhabditis Genetics Center	PD4482
Golgi apparatus membrane (vha-6p:mans:GFP + Cbr-unc-119(+))	Caenorhabditis Genetics Center	RT1315
Yolk (vit2:GFP)	Caenorhabditis Genetics Center	RT130
peroxisome membrane (hjIs73 [vha-6p:GFP:daf-22 + C. briggsae unc-119(+)])	Caenorhabditis Genetics Center	VS11
lysosome related organelles (gut granules) (hjIs9 [ges-1p:glo-1:GFP + unc-119(+)])	Caenorhabditis Genetics Center	VS17
lysosome membrane (pwIs50 [lmp-1:GFP + Cbr-unc-119(+)])	Caenorhabditis Genetics Center	RT258
late endosome membrane (pwIs170 [vha6p:GFP:rab-7 + Cbr-unc-119(+)])	Caenorhabditis Genetics Center	RT476
Bacterial and virus strains		
Escherichia coli OP50	Caenorhabditis Genetics Center	Cat# OP50
Escherichia coli $OP50^{\Delta PPK\Delta PPX}$	Datsenko and Wanner[34]	OP50 ΔPPKΔPPX
Escherichia coli MG1655	Blattner et al.[35]	MG1655 (genotype: *F*− λ− rph-1 ilvG rfb-50)
Escherichia coli $MG1655^{\Delta PPK}$	Gray et al.[21]	MG1655 Δppk-749

(*Continued on next page*)

Continued

REAGENT or RESOURCE	SOURCE	IDENTIFIER
Software and algorithms		
FIJI (ImageJ) (RRID: SCR_003070) version 1.53c	http://imagej.nih.gov/ij Schindelin et al.[36]	FIJI
GraphPad Prism v 9.5.1 (733)	GraphPad	Prism
Excel	Microsoft	Microsoft Office Professional Plus 2016
LAS X version 3.3.0.16799	Leica	LAS X
Other		
Cellpath Stainless-steel Reusable Base Molds	Fisher Scientific	cat # 22-222-033
3D printed pronged molds (resin printed due to needing tight tolerances in shape)	This study	Contact Ellen Quarles for files
3D printed centrifuge adaptors (filament printed due to larger size and strength needed under centrifugation)	This study	Contact Ellen Quarles for files
Wide-field microscope on SP8 base	Leica	Thunder
Cryostat	Leica	3050s
SP8 confocal microscope (DMI8 base)	Leica	SP8

EXPERIMENTAL MODEL AND STUDY PARTICIPANT DETAILS

Strains

All worm strains were obtained from the Caenorhabditis Genetics Center. Wild type bacterial strains (OP50 and MG1655) came from the Caenorhabditis Genetics Center. Introducing the null mutations in OP50 (OP50$^{\Delta ppk\Delta ppx}$) has been conducted as described by K. A. Datsenko, B. L. Wanner, 2000.[34] Null mutation in MG1655 has been described in Gray et al., 2014.[21]

Culturing *C. elegans*

Worms were grown on nematode growth media (NGM) agar with appropriate antibiotics at 20°C. Plates were seeded with overnight cultures of OP50 or MG1655 bacteria, and worms were always kept in food-excess conditions unless otherwise stated. Age synchronization was accomplished with the bleach method (Wormbook.org, "Harvesting asynchronous culture and seeding synchronous cultures"). Hermaphrodites were used for all experiments. Worms were removed from plates by washing with PBS buffer.

METHOD DETAILS

Preparation of cryomolds

Gelatin solution (10% D-sucrose, 10% bovine gelatin, 1x PBS no calcium/magnesium, 1 drop per ~10 mL, blue or green food coloring) was prepared and heated in a water bath at 37°C–42°C with occasional mixing until completely melted. Unused gelatin solution was stored at 4°C for up to two weeks. Into each metal cryomold (Cellpath Stainless-steel Reusable Base Molds, Fisher Scientific, cat # 22-222-033) the gelatin solution was pipetted until the mold was halfway filled. Immediately, the 3D printed pronged mold was added and centered, and the entire apparatus was kept level, and allowed to cool at 4°C until the gelatin had solidified. Bubbles were avoided, and removed by pipetting or running a flame briefly over the liquid. The 3D printed pronged molds were removed by gently rocking them and slowly pulling them away from the gelatin. These were then gently wiped clean and stored at room temp. The prepared cryomolds were either used immediately or stored at 4°C in a sealed plastic bag for up to one week to prevent drying.

Freezing worms in cryomolds

200 - 10,000 worms were washed off NGM plates using M9 media or PBS. Adult worms were allowed to settle by gravity for up to 2 min, then the supernatant was removed by decanting or pipetting. The pellet of worms was washed twice more with M9 or PBS. Then, 2 mL of 4% v/v paraformaldehyde (PFA) in PBS was added to the worm pellet. Worms were incubated at room temperature in the PFA solution for 10 min and gently mixed by tube inversion every 2–3 min. The PFA serves two purposes: to kill the worms, and to help maintain structural integrity of the worms throughout the cryosectioning process. PFA was removed, and the worm pellet was washed with 0.01% v/v Triton ×100 in PBS for 10 min. This step is necessary to maintain smooth cuticle structure during sectioning, and to help the worms not stick to the tube walls. Worms were centrifuged at 500*g for 1 min at room temperature, and the supernatant was removed to allow easy pipette access to the pellet. Worms were then pipetted with a 1000 μL tip, with the end cut off by several mm to facilitate easy and gently moving of the worms, into one or more wells of the prepared cryomolds. The worms settle to

the bottom of the cryomolds in seconds. Then, we used a 2–10 μL pipette tip to pipette away the supernatant from the cryomold wells using a stereoscope to help visualize the worms. This is made easier by holding the tip extremely close to the gelatin at the sides of the wells, close enough that the adult worms cannot get sucked into the tip. Once the supernatant was fully removed an embedding compound commonly used to support sectioning of frozen tissue (O.C.T., Optimal Cutting Compound, purchased from Fisher Scientific) was added to the wells, filling them approximately halfway. A 2–10 μL pipette tip was used to gently stir the worms around in the O.C.T. to ensure they were entirely covered by the compound, and that they were evenly distributed in the well. Care must be taken to not damage the gelatin mold in this step. Then, O.C.T. was added again to top off the wells, and to fill the cryoblocks with 0.5 cm or more height of O.C.T. over the gelatin layer. All blocks were weighed and balanced using O.C.T. The cryomolds were centrifuged in 3D printed (filament) centrifuge adaptors designed to hold 2 metal cryomolds each, sized to fit into standard plate holders. Centrifugation was done at 4°C or room temperature for 8 min at 1500*g, in swinging plate holders. The blocks were then visually inspected to ensure all worms were only in the bottom of the wells, and evenly distributed within each well. If not, they were remixed, and re-balanced, and re-spun. Completed blocks were flash frozen in a dry ice-EtOH slurry. Frozen blocks were marked with permanent marker to delineate the orientation of the block for future cutting and removed from the metal molds by inverting them and hitting the metal molds against a napkin-covered countertop to dislodge the block. The blocks were wrapped in labeled paper and stored at −80C until sectioning.

Cryosectioning

Blocks were allowed to warm up to −20°C, and adhered to cryostat chucks with the non-gelatin side attached to the chuck by O.C.T. The food coloring in the gelatin allows easy visualization of the alignment of, and distance to, the white circles of the wells which become more apparent as further layers of gelatin are removed. This also allows for a clear reference of the angle of the cryosections and allows the user to correct that alignment before the bottom of the wells (where all the worms are present) gets sectioned. Blocks were cryosectioned on a Leica 3050s cryostat at 10–12 μm per slice. Thicker and thinner sections are also possible. Thicker sections allow for easier handling of the section, and more stainable/image-able tissue sections, but they have reduced image clarity due to the light refracting through the tissues when using standard confocal or wide field microscopy. Thinner sections give clearer fluorescent images but can be difficult to handle and reduce the z-depth of the tissue, which can be an issue when generating z stack images. Sections were dried immediately after being applied to the slides, on a slide warmer set to 30°C for 10–30 min. The slides were either stained the same day or the subsequent day after remaining in a dark box overnight at room temperature. Freezing the slides at −80°C before staining did not seem to affect *Ec*PPXbd-eGFP signal intensity or distribution.

Purification of fluorescent probes, ScPPX and DPP1

The creation of the plasmids containing mCherry-*Ec*PPXbd, eGFP-*Ec*PPXbd and ScDPP1 was described previously.[15,24,33] Purification of these and the HIS-tagged mCherry, eGFP, scPPX and *Sc*DPP1 proteins was performed using a nickel-NTA column (Qiagen, Germany). In short, after 4-6h expression, *E. coli* strains transformed with each of the plasmids except *Sc*DPP1 were lysed in lysis buffer (40 mM Tris, 10mM sodium phosphate buffer, 10% v/v glycerol, 10 mM $MgCl_2$, pH 8.0) with cOmplete protease inhibitor cocktail, DNASE I, and RNase A (all from Milipore-Sigma). Samples were sonicated, centrifuged, and the supernatant was loaded onto HisTrap columns (Sigma-Aldrich). Proteins were eluted with imidazole, dialyzed against 20 mM NaP, 50 mM KCl, 10% v/v Glycerol, pH 7.5 and stored at −70 °C at 1 mg/mL. *Sc*DDP1 protein was isolated by lysing cells in lysis buffer (50 mM sodium phosphate buffer, 500 mM NaCl, 10 mM imidazole, with 1 mg/mL lysozyme, 2 mM $MgCl_2$, and 50 U/mL Benzonase). Cells were incubated on ice for 30 min, then sonicated and centrifuged to pellet cell debris. Lysates were loaded onto NiNTA columns and eluted with imidazole (pH 8.0). Protein was dialyzed against 20 mM Tris-HCl (pH 7.5), 50 mM KCl, 30% (v/v) glycerol, and stored at −70 °C at 1 mg/mL. The purity of the proteins was analyzed by reducing SDS PAGE followed by Coommassie staining (Figure S3C).

Staining and immunofluorescence

The wells of the cryosections are visible on the slide as they show up as clear circles against a colorful gelatin background. To track the samples, we used a permanent marker and labeled the positions on the side of the glass slide that did not contain the worms. On the same side of the slide as the worms, we used a PAP pen (Electron Microscopy Sciences, # 106-94-5) to corral the staining fluids away from the top label and bottom edge of the slides.

EcPPXbd-eGFP staining - Briefly, the sections were fixed with 4% v/v PFA in PBS for 10 min, followed by 3x washing with PBS for 5 min each. Permeabilization of the tissues was accomplished by incubation with 0.3% v/v Triton ×100 in PBS for 10 min (longer incubation times allowed DNA to leak out of nuclei, shorter times did not allow for complete *Ec*PPXbd-eGFP staining in the intestine). Sections were washed three more times with PBS, and incubated in blocking buffer (2% BSA, 22.52 mg/mL glycine, 1x PBS) for 30–60 min. Blocking buffer containing either 10 μg/mL *Ec*PPXbd-eGFP (or *Ec*PPXbd-mCherry) or 10 μg/mL eGFP (or mCherry) was added to the sections, which were incubated for 4 h to overnight in a humid, dark chamber. The sections were subsequently washed with PBS three more times, and incubated for 10 min with 0.1 μg/mL DAPI in PBS with occasional gentle rocking. This was followed by two more washes with PBS. A 1.5 size coverglass (Corning) was mounted using Prolong Gold. Slides were sealed with clear nail polish (Sally Hansen Hard as Nails Xtreme Wear, Invisible) and stored at 4°C in the dark until imaging. All PBS-containing steps were conducted at room temperature, and with gentle rocking/mixing every 1–3 min, except for blocking and staining steps, which were allowed to remain still.

Oil Red O Staining - Freshly cryosectioned, air dried sections were washed with DI water two times, briefly. Polypropylene glycol (100%) was added for 2 min, then drained off the slides. The sections were then incubated in either 100% polypropylene glycol (controls) or Oil Red O working solution (0.5% Oil Red O in 100% polypropylene glycol, heated to 95C, filtered, and stored at room temperature) for 8 min at 60°C. Slides were destained in 85% polypropylene glycol 3 min at room temperature. Finally, sections were washed twice briefly in DI water. The sections were then stained with *Ec*PPXbd-eGFP or GFP as above.

Antibody staining - Sections were treated as above for *Ec*PPXbd-eGFP, with the following additions. For mouse anti-*C. elegans* RME-1 staining: After the blocking step, sections were incubated with 10 μg/mL anti-RME-1 or no primary antibody (with and without *Ec*PPXbd-mCherry or mCherry) overnight in a dark, humid chamber at room temperature. Sections were washed with 1x PBS three times, then incubated with anti-mouse Alexa Fluor 488 secondary antibody, at 1:1000 dilution in blocking buffer, for 1 h at room temperature. Sections were then washed again with 1x PBS three times, and mounted as above. For mouse anti-*C. elegans* LMP-1 staining: Same as anti-RME-1 staining, except a heat-induced antigen retrieval (HIAR) step was added just prior to the blocking step. We accomplished HIAR by adding 10 mM sodium citrate, pH 7.0 pre-warmed to 95°C to the sections on a hot (95°C) block for 60 s. The slides were then immediately drained and room temperature 1x PBS was used to wash the slides twice. The rest of the protocol is as above for anti-RME-1.

Fluorescence microscopy

Widefield images were captured using a Leica THUNDER (widefield microscope) on a T8i inverted base, with an HC PL APO 40x/1.3 NA oil objective (catalog number 11506358). Leica Navigator software was used to run Tile Scan and stitching functions. THUNDER Instant Computational Clearing (ICC) method was run for background and blur reduction. Focusing over the tile scanned areas was achieved by adding Focus Points within the area to be scanned using Navigator. An LED8 was used to excite all fluorophores (DAPI, Ex: 395 nm, Em: 460/80 nm; EGFP, Ex: 488 nm, Em: 535/70 nm; mCherry, Ex: 555 nm, Em: 590/50 nm), and the CYR7101, DFT51010, and EMP_BF filter cubes were used for emission. Images were captured with an Andor Zyla sCMOS camera.

Confocal images were captured using a Leica SP8 scanning confocal microscope (Leica GmbH, Mannheim Germany) on a DMI8 microscope base, using LAS X software, and an HC PL APO 100x/1.40 oil objective (Leica 11506378). A 405 nm diode laser, and multi-line white light laser were used for excitation (set to 488 and 585 nm). PMT detectors were used for spectral detection (DAPI: 410–480 nm, EGFP: 495–560 nm, mCherry: 600–675 nm). A transmitted light PMT, with the 405 nm laser, was used to capture a brightfield image. Control images without antibodies or *Ec*PPXbd-bound fluorophores are in Figures S1B–S1F.

Measurement of fluorescence intensity

Image analysis was performed using FIJI (ImageJ 1.53t, Java 1.8.0_172). For each image, a composite of the DAPI (for DNA) and brightfield channels was made and used to define regions of interest (ROIs) using a rectangle of defined width/height that would cover the width of the worms (150 px), and a height of 115 px. These were placed on worms along areas with visible gut cells covering the entire width of the worm, as identified by the nuclear shape and size. (Gut cell nuclei are much larger than gonadal nuclei.) The saved ROIs were then used to measure eGFP or mCherry fluorescence intensity on the appropriate tiff channels, and a large non-worm background ROI intensity was subtracted from each measurement per image. In worms in which multiple ROIs could be made, up to 3 were made and averaged.

Food removal and recovery

Age-synchronized D1 adult N2 worms, grown on $OP50^{WT}$ bacteria were washed with M9 media three times to remove bacteria. The worms were then re-distributed onto either NGM plates containing $OP50^{WT}$ or no bacteria. After 4 h at 20°C, fed and starved worms were cryoblocked. The remaining starved worms were transferred onto $OP50^{WT}$-containing plates to recover from starvation for 1, 2, 4, or 24 h and then cryoblocked.

Enzyme digestion used in Figure S3

Sections were treated as for *Ec*PPXbd-eGFP, with the following additions: After permeabilization with Triton X-100, sections were washed in 1x PBS, 3x, 5 min each. The sections then underwent Heat Induced Antigen Retrieval (HIAR) to allow for polyP-*Sc*PPX1 interaction post fixation. To the sections, we added 10 mM sodium citrate, pH 7.0 pre-warmed to 95°C, on a hot (95°C) block for 60 s. The slides were then immediately drained and room temperature 1x PBS was used to wash the slides twice. Then the sections were washed 1x, 5 min at RT in *Sc*PPX1 buffer (20 mM Tris-HCl pH 7.5, 5 mM $MgCl_2$, 50 mM ammonium acetate). The *Sc*PPX1 with heat-inactivated DDP1, DDP1 with heat-inactivated *Sc*PPX1, *Sc*PPX1 with DDP1, or both enzymes heat-inactivated were added to the sections at 5 ng/mL in *Sc*PPX1 buffer. These were incubated in a dark, humid chamber at 37C for 2 h. Then the sections were washed 3x with 1x PBS, 5 min each, and the *Ec*PPXbd-eGFP staining procedure was continued as described in the main text methods starting at the blocking step.

QUANTIFICATION AND STATISTICAL ANALYSIS

GraphPad Prism 9 was used to perform statistical analysis and to produce graphs. Specific tests and post-hoc analyses are described in figure legends. Unless otherwise stated, dots within graphs represent biological replicate experiments, and data are presented with a bar indicating the mean ± SEM. P-values are listed on the graphs for comparisons made. Kruskal-Wallis tests were used instead of ANOVA because at least one group in each comparison had unequal variance with the rest of the groups, and because some groups violated an assumption of a normal distribution. Number of worms used for measurements ranged from 20 to 50 per group.

Cell Reports Methods, Volume *4*

Supplemental information

Cryosectioning and immunofluorescence of *C. elegans* reveals endogenous polyphosphate in intestinal endo-lysosomal organelles

Ellen Quarles, Lauren Petreanu, Anjali Narain, Aanchal Jain, Akash Rai, Joyful Wang, Bryndon Oleson, and Ursula Jakob

SUPPORTING FIGURES

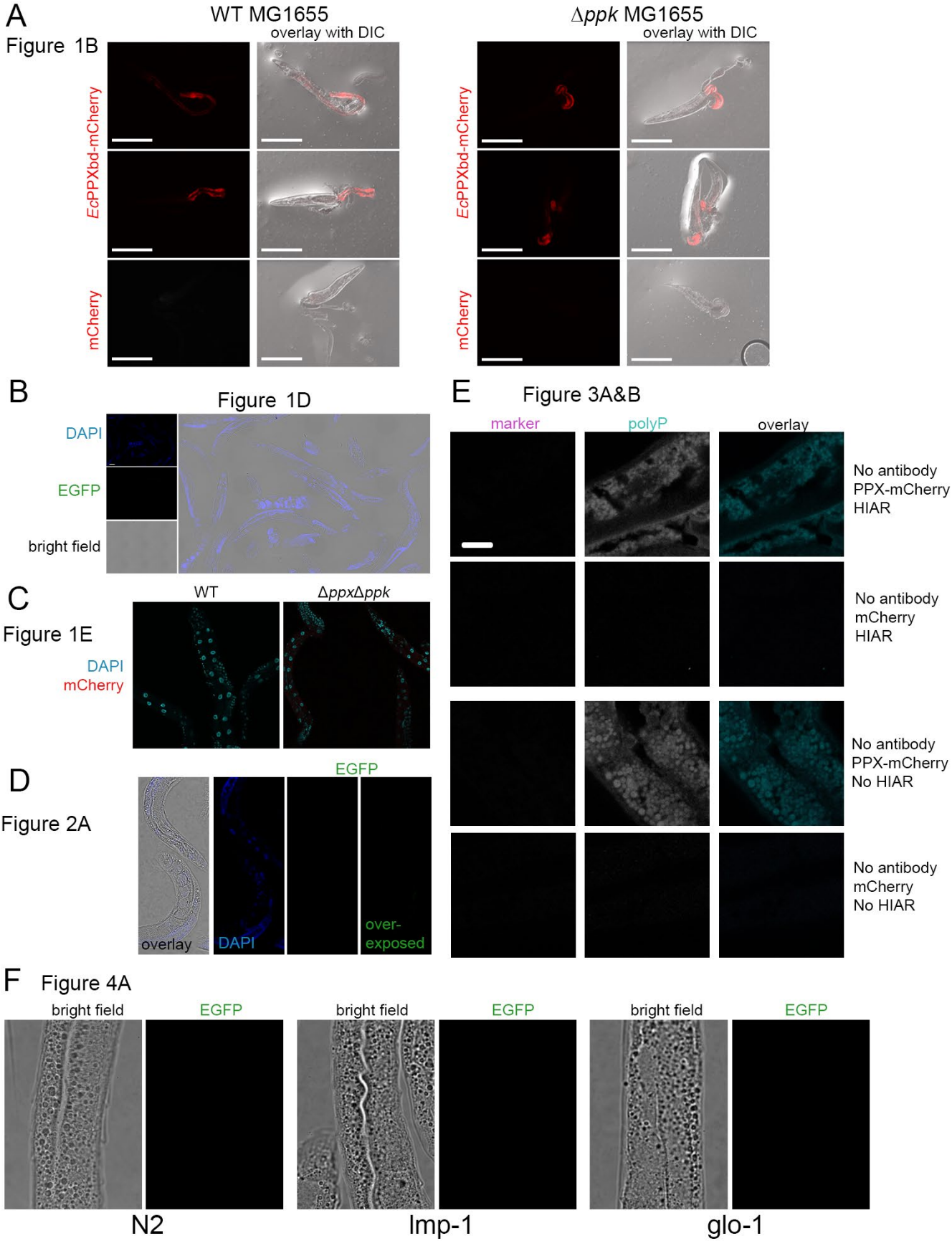

Supporting Figure 1. Example images of control conditions for all main text Figures. A) Higher resolution images of Figure 1B: Dissected adult N2 worms, stained with *Ec*PPXbd-mCherry, and the DIC image, shown in overlay. Scale bars are 200 µm. The worms were raised on either wild-type MG1655 *E. coli*, or a *ppk* deletion mutant. Bottom row of each bacteria type: worms stained with mCherry alone. B) *Ec*PPXbd-EGFP control stained sample for Figure 1D. C) mCherry control stained samples for Figure 1E. D) EGFP control stained sample for Figure 2A. E) Four staining-control conditions shown from top to bottom for Figure 3A&B (No antibody used on N2 wildtype sample, +/- PPX-mCherry vs mCherry staining, +/- Heat Induced Antigen Retrieval which was used for lmp-1 antibody testing). Scale bar is 8.5 microns. Images are zoomed out to show clear lack of polyP-related signal. F) Bright field and EGFP channels for N2, lmp-1KO, and glo-1KO samples serving as controls for Figure 4A. All images are brightness corrected to the same level as the polyP-channels in the figures in the main text.

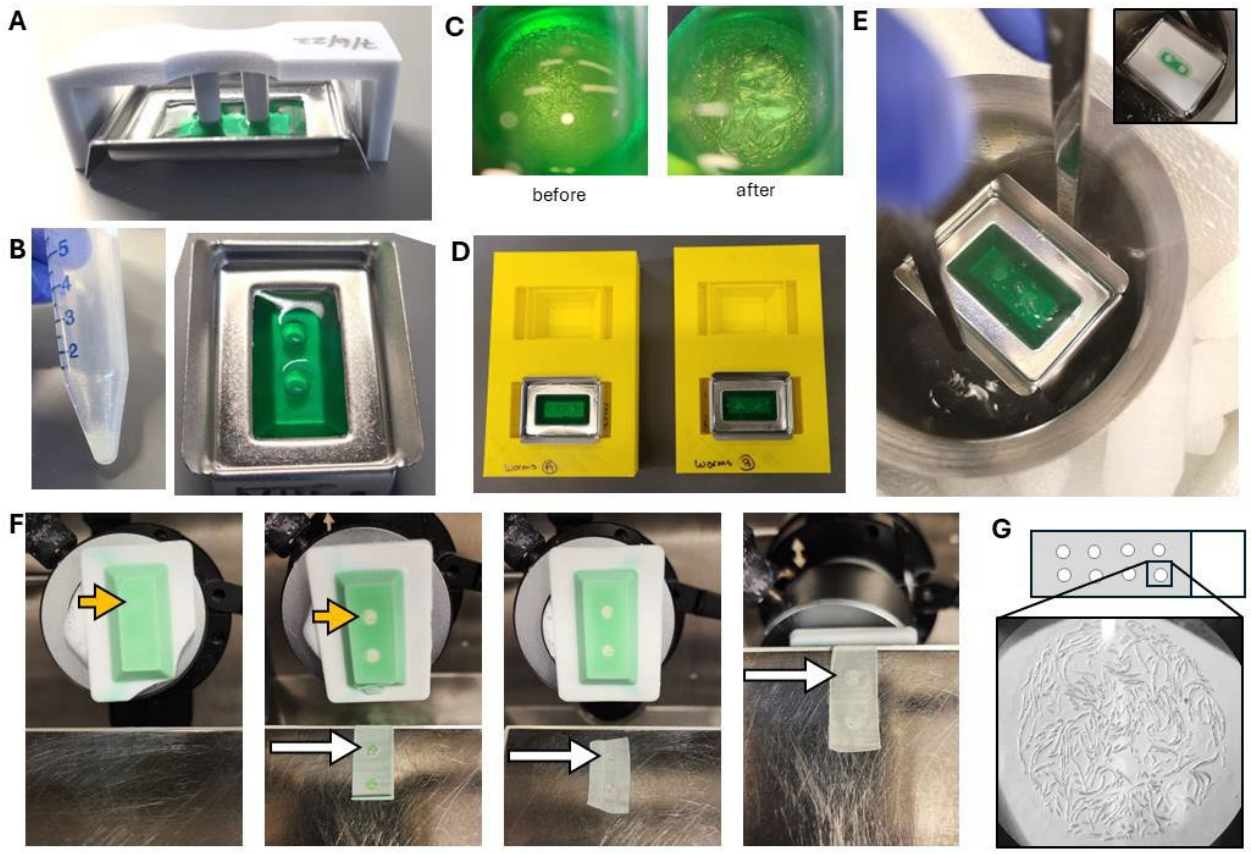

Supporting Figure 2. Images detailing STAR*Methods sections for Cryomold preparation, Freezing worms in cryomolds, and Cryosectioning. A) 3D-printed mold inserted into gelatin-solution in metal cryomold. B) Densely packed worms in PBS, left, to be added to the individual wells left by after 3D printed mold removal from gelatin solution, right. C) After PBS+ worms are added to the wells ("before"), the worms immediately sink to the bottom of the well ("after"). After removing the PBS, the worms are still apparent in the well. D) Metal cryomolds with worms and gelatin solution are filled with O.C.T., placed into centrifuge adaptors, and spun down to ensure worms are aligned with the bottom of the gelatin wells. E) Immediately after removal from the centrifuge, the metal cryomolds are flash frozen by dipping them into an ethanol-dry ice slurry, taking care not to submerge the O.C.T. Insert – the cryomolds are removed from the slurry once most of the volume of O.C.T. has frozen over, as the remainder of the freezer will happen on dry ice. F) Once removed from the metal cryomolds, the frozen blocks are added to a cryostat chuck, keeping the bottom of the wells toward the user. Those wells are only barely visible before any cuts are made (leftmost image) but become highly contrasted from the gelatin when enough of the bottom layers of the block are removed (yellow arrows indicate similar well positions). The slices that come of the block show the well positions more clearly as the user gets closer to the location of the worms, turning from darker-than-surrounding gelatin just below the worm position, to white as the O.C.T. and worm area is entered. Slices with and without worms look the same so long as the O.C.T. is present (white arrows indicate same well position before O.C.T. begins, at the beginning of the worm layer, and well past the worm layer height, from left to right). G) After the slices are mounted on a slide and dried, the O.C.T. and gelatin areas become clear, and the worm material is visible by eye and stereomicroscope.

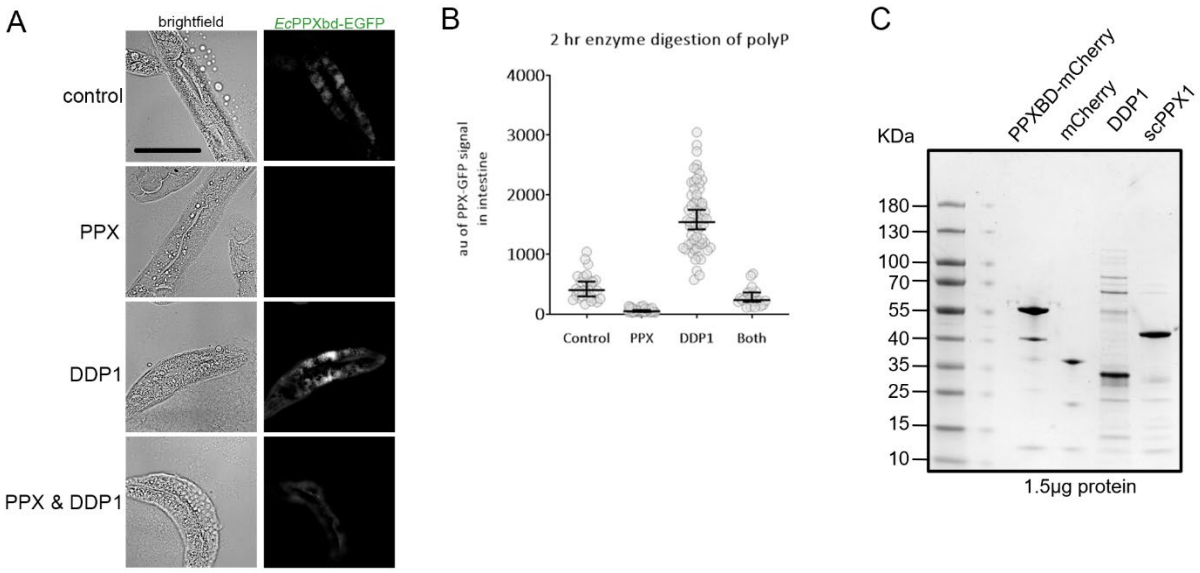

Supporting Figure 3. *Ec*PPXbd-GFP signal is specific to PPX-digestible material, related to STAR*Methods titled Enzyme Digestion and Purification of Fluorescence Probes. A) Sample images of *Ec*PPXbd-GFP signal and bright field after treating slides with *Sc*PPX1, the endopolyphosphatase DDP1, both heat-inactivated enzymes ("control"), or both active enzymes. Scale bar is 100 µm. B) Quantification of *Ec*PPXbd-GFP signal after two-hour treatment of slides +/- PPX, +/- DDP1. Each circle represents one worm intestine. Lines: mean +/- SEM. C) Protein gel of probes and enzymes used in this study. From left to right, the lanes are protein ladder, empty well, *Sc*PPXbd-mCherry, mCherry, DDP1, and PPX1. Coomassie stain was used to detect total protein. 1.5 µg protein was loaded per well.

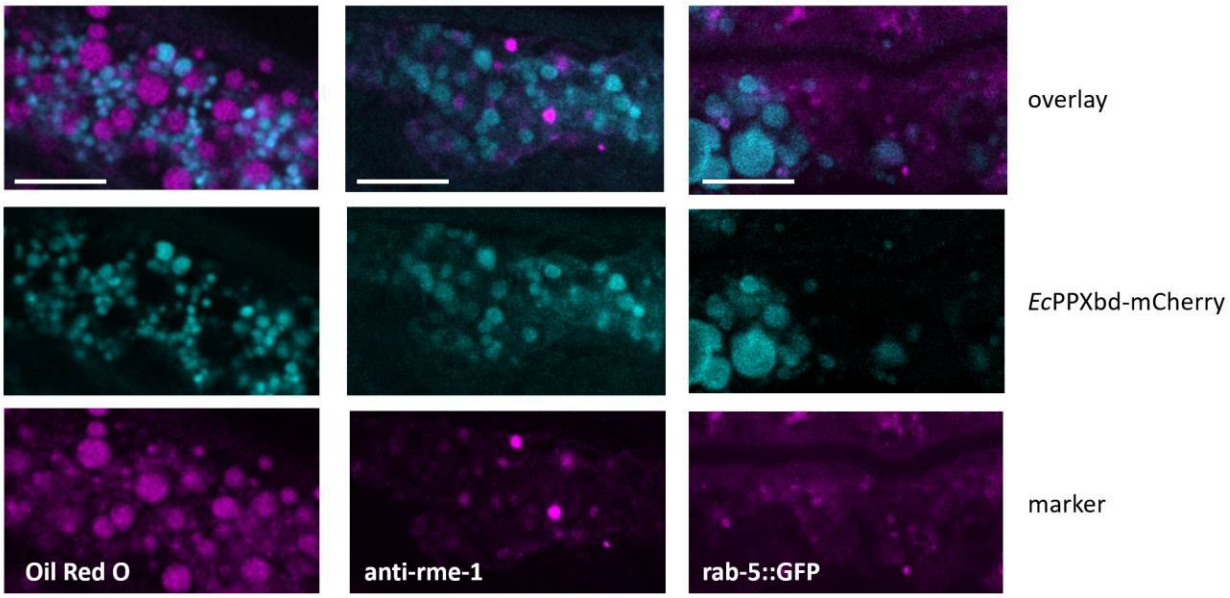

Supporting Figure 4. *Ec*PPXbd-mCherry+ puncta are not surrounded by or co-localized with markers of lipid droplets, recycling endosomes, or early endosomes, related to Figure 3. Shown are images of representative D1 worm intestinal cells, expressing the listed markers of lipid droplets (Oil Red O), recycling endosomes (anti-rme-1 with AF488 secondary antibody), and early endosomes (rab-5::GFP), stained with *Ec*PPXbd-mCherry, and overlays. Scale bar is 10 μm. All markers are pseudocolored magenta, and all *Ec*PPXbd-mCherry panels are pseudocolored cyan.

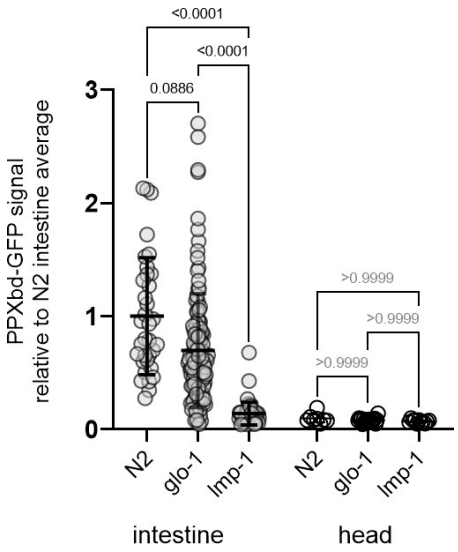

Supporting Figure 5. Knock-out of glo-1 or lmp-1 from the intestine does not change polyP signal in the head, related to Figure 4. Relative fluorescence of *Ec*PPXbd-eGFP signal in intestine and head. Each circle is one worm. Kruskal-Wallis test with Tukey post-hoc. Lines are mean+/-SD. *P*-value is shown for each comparison made.